Available online at www.sciencedirect.com
ScienceDirect
Electrochemistry Communications 9 (2007) 1041–1046
electrochemistry communications
www.elsevier.com/locate/elecom

$Li_{0.93}[Li_{0.21}Co_{0.28}Mn_{0.51}]O_2$ nanoparticles for lithium battery cathode material made by cationic exchange from K-birnessite

Yoojin Kim [a], Youngsik Hong [b], Min Gyu Kim [c], Jaephil Cho [a,*]

[a] Department of Applied Chemistry, Kumoh National Institute of Technology, Gumi, Republic of Korea
[b] Department of Science Education, Seoul National University of Education, Seoul, Republic of Korea
[c] Beamline Research Division, Pohang Accelerator Laboratory, Pohang University of Science and Technology, Pohang, Republic of Korea

Received 29 November 2006; received in revised form 14 December 2006; accepted 14 December 2006
Available online 25 January 2007

Abstract

$Li_{0.93}[Li_{0.21}Co_{0.28}Mn_{0.51}]O_2$ nanoparticles with an R-3m space group is hydrothermally prepared from $Co_{0.35}Mn_{0.65}O_2$ obtained from an ion-exchange reaction with K-birnessite $K_{0.32}MnO_2$ at 200 °C. Even at a hydrothermal reaction temperature of 150 °C, the spinel (Fd3m) phase is dominant, and a layered phase became dominant by combining an increase in the temperature to 200 °C with an increase in lithium concentration. The as-prepared cathode particle has plate-like hexagonal morphology with a size of 100 nm and thickness of 20 nm. The first discharge capacity of the cathode is 258 mAh/g with an irreversible capacity ratio of 22%, and the capacity retention after 30 cycles is 95% without developing a plateau at ~3 V. Capacity retention of the cathode discharge is 84% at 4C rate (=1000 mA/g) and shows full capacity recovery when decreasing the C rate to 0.1 C.

Keywords: Nanoparticles; Cationic exchange; K-birnessite; Layered structure; Rate performance; Hydrothermal reaction

1. Introduction

Since the study in which Delmas et al. investigated ion-exchange reactions and extraction and insertion in layered transition metal oxide bronzes below 300 °C [1], many attempts have been made to prepare layered $LiMn_{1-x}M_xO_2$ that primarily involve the use of aqueous solutions [2–4]. The products obtained by these methods, however, have stoichiometries which differ from $LiMn_{1-x}M_xO_2$, contain water and a proton, and of are poor crystallinity or do not maintain their structure during cycling. Armstrong et al. reported that anhydrous and stoichiometric $Li_{0.5}MnO_2$, which is analogous to $LiCoO_2$, was obtained by ion-exchange from $NaMnO_2$ [5]. $LiMnO_2$ was obtained by refluxing $NaMnO_2$ with an excess of LiCl or LiBr in *n*-hexanol at 145–150 °C for 6–8 h. However, a displacement of Mn^{3+} ions into the lithium layers occurs, forming regions with a spinel phase, as evidenced by voltage plateaus at 3 and 4 V. However, 10 mole% Co and Ni doping in $LiMnO_2$, i.e., $Li_{0.85}M_{0.9}Co_{0.1}O_2$ (M = Ni and Co) showed no evidence of a monoclinic distortion arising from the Jahn–Teller active Mn^{3+} ion [6,7]. These cathode materials transformed to a spinel structure with cycling, but the transformation was slowed, and the resulting materials showed improved capacity retention. The synthetic methods described so far have a common point in using $NaMnO_2$ as a precursor phase for ion-exchange [8]. A method similar to these was reported by Tabuchi et al., and the synthesis of monoclinic $LiMnO_2$ from Mn_2O_3 and mixed alkaline solutions such as LiOH(LiCl)–KOH at 220 °C by hydrothermal reactions was obtained [9]. This material also showed a spinel phase transition during cycling. On the other hand, layered $LiMO_2$ (M = Co, Ni) compounds were synthesized at less than 160 °C with an air pressure of 60 bars from MOOH/LiOH and a

* Corresponding author. Tel.: +82 54 478 7824; fax: +82 54 478 7710.
E-mail address: jpcho@kumoh.ac.kr (J. Cho).

1388-2481/$ - see front matter © 2006 Elsevier B.V. All rights reserved.
doi:10.1016/j.elecom.2006.12.020

H_2O/H_2O mixture [10]. However, the Li_xNiO_2 obtained showed 20 mole % Ni ions in the lithium sites and a reversible capacity of less than 80 mAh/g between 4.1 and 3 V.

Recently, Xu et al. reported that layered $Li_x[Li_y$-$Ni_nMn_m]O_2$ with a layered structure could be obtained through the hydrothermal treatment of mixed layered $Ni(OH)_2$ and H^+-form of birnessite manganese oxides in a concentrated LiOH solution at 200 °C [11]. They reported that the initial discharge capacity of the as-prepared cathode is only 120 mAh/g between 2 and 4.2 V, and no other voltage profiles were shown.

Birnessite consists of layers of edge- and corner-linked MnO_6 octahedra with water molecules and alkali metal cations in the interlayer voids [12–15]. A generalized elemental composition of birnessite is $A_xMnO_{2\pm y} \cdot H_2O$, where A is an alkali metal cation, and the average oxidation state of the mixed-valence manganese normally falls between 3.6 and 3.8, which represents a predominance of Mn^{4+} with minor amounts of Mn^{3+} [16–18].

In this study, we report the preparation and electrochemical characterization of layered $Li_{0.93}[Li_{0.21}Co_{0.27}$-$Mn_{0.51}]O_2$ cathode materials prepared from K-birnessite precursor by using a hydrothermal reaction at 200 °C. The layered cathode nanoparticle can deliver a reversible capacity of 258 mAh/g.

2. Experimental

2.1. Synthesis of K-birnessite

A solution containing 3.26 g of $KMnO_4$ and 100 ml of distilled water was slowly stirred for 30 min at 40 °C and added to 0.82 g of fumaric acid which resulted in a rapid, exothermic reaction, forming a brown gel. This gel was further annealed at 400 °C and 700 °C for 6 h and 12 h, respectively, and the resulting dark black powders were washed with water three times, followed by vacuum-drying at 150 °C overnight. Inductively coupled plasma mass spectrometry (ICP-MS) and a CHS elemental analysis of the sample confirmed $K_{0.32}MnO_2$, and the average Mn oxidation state was 3.67.

2.2. Synthesis of $Co_{0.35}Mn_{0.65}O_2$

As-prepared K-birnessite was mixed with $CoCl_2 \cdot 6$-H_2O:$K_{0.32}MnO_2$ with a weight ratio of 5:1 in 100 ml of distilled water, stirred for seven days at room temperature, and finally washed with water four times in order to remove residues that did not participate in the reaction. Finally, the powder was vacuum-dried at 200 °C for 24 h, and its composition was $Co_{0.354}Mn_{0.656}O_2$ based upon an ICP-MS analysis.

2.3. Synthesis of $Li_{0.93}[Li_{0.21}Co_{0.27}Mn_{0.51}]O_2$

$LiOH \cdot H_2O$ and $Co_{0.35}Mn_{0.65}O_2$ combined with weight ratios of 1:1, 2:1, and 4:1 were mixed in 50 g of distilled water, and kept at 150 °C and 200 °C for 1 h to 24 h in an autoclave. The as-prepared powders were rinsed with water, and dried under vacuum at 200 °C. The sample prepared with a weight ratio of 1:1 had a stoichiometry of $Li_{0.51}Co_{0.35}Mn_{0.65}O_2$, while the sample with a weight ratio of 4:1 had a $Li_{0.93}[L_{0.21}Co_{0.28}Mn_{0.51}]O_2$ stoichiometry.

2.4. Characterization

Powder X-ray diffraction measurements were carried out using a Rigaku DMax/2000PC with a Cu-target tube. Inductively coupled plasma-mass spectroscopy (ICP, ICPS-1000IV, Shimadzu) was used to determine the metal contents. A field-emission transition electron microscope (FE-TEM) (JEOL 2100F), operating at 200 KV, was used for investigating the microstrcure of the samples. The Co and Mn K-edge X-ray absorption spectra were carried out on the BL7C (Electrochemistry) beamline at the Pohang Light Source (PLS), which is a third generation synchrotron radiation source, in the 2.5 GeV storage ring with a ring current of 120–170 mA. A Si(1 1 1) double crystal monochromator was used to monochromatize the X-ray photon energy. Higher order harmonic contaminations were eliminated by detuning the monochromator in order to reduce the incident X-ray intensity by ~30%. The incident X-ray intensity was monitored using pure nitrogen gas-filled ionization chambers. The spectroscopic data was collected in transmittance mode.

2.5. Electrochemical characterization

Coin-type half-cell tests were conducted, using samples at different C rates between 2 and 4.8 V, using the same 0.1 C (=25 mA/g) rate for charging at 21 °C. Cathodes for battery test cells were made of the active material, super P carbon black (MMM, Belgium), and polyvinylidene fluoride (PVdF) binder (Solef) in a weight ratio of 80:10:10. A cathode-slurry was prepared by thoroughly mixing a *N*-methyl-2-pyrrolidene (NMP) solution with the PVdF, the carbon black, and the powdery cathode-active material. Electrodes were prepared by coating the cathode-slurry onto an Al foil, followed by drying at 130 °C for 20 min. Coin-type battery test cells (size 2016R), containing a cathode, a Li metal anode, and a microporous polyethylene separator, were prepared in a helium-filled glove box. The electrolyte used was 1.03 M $LiPF_6$ with ethylene carbonate/diethylene carbonate/ethyl-methyl carbonate (EC/DEC/EMC) (3/3/4 vol%) (Cheil Ind., Korea).

3. Results and discussion

Fig. 1 shows XRD patterns of K-birnessite ($K_{0.32}MnO_2$) prepared by a sol–gel method and $Co_{0.35}Mn_{0.65}O_2$ prepared by using K-birnessite. The patterns were dominated by two major peaks at ~12.5° (0 0 2) and ~25° (2 1 2) scattering angles, which are signatures of synthetic birnessite materials, and showed preferred orientation along the *c*-axis [13]. The

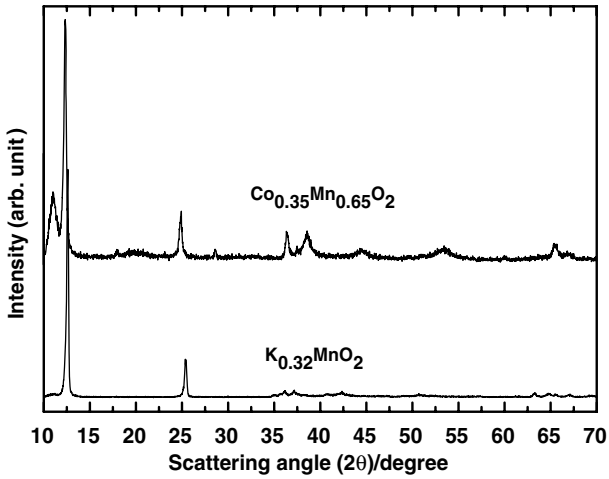

Fig. 1. XRD patterns of K-birnessite ($K_{0.32}MnO_2$) and $Co_{0.35}Mn_{0.65}O_2$.

broadening of the two major peaks after the Co ion-exchange indicated increased disordering in the cations between the layers or decreased crystallinity. Fig. 2 shows XRD patterns of the $Li_xCo_{0.35}Mn_{0.65}O_{2+z}$ prepared at different $LiOH \cdot H_2O$ and $Co_{0.35}Mn_{0.65}O_2$ concentrations ($Co_{0.35}Mn_{0.65}O_2$: $LiOH \cdot H_2O$) (wt %)(1:1, 1:2, and 1:4) at 150 °C and 200 °C. The stoichiometry of the sample prepared at 150 °C was $Li_{0.51}Co_{0.35}Mn_{0.65}O_2$ (sample A), and showed the formation of a spinel phase under conditions when the weight ratio of $Co_{0.35}Mn_{0.65}O_2$ to $LiOH \cdot H_2O$ was 1:2 at 200 °C. The XRD patterns showed a mixed phase that consisted of a major layered phase with a space group of R-3m and a minor spinel phase (sample B). When the $LiOH \cdot H_2O$ concentration increased to four-fold and the temperatures was maintained at 200 °C, a major layered hexagonal phase was observed and the peaks at ~21–25° were also observed (sample C). These peaks are attributed to the superlattice ordering of Li and Mn in the transition metal containing layers and have been observed Li_2MnO_3-based oxides [19–22]. The ICP-MS results showed the formation of $Li_{1.5}Co_{0.35}Mn_{0.65}O_{5.15}$ and, when normalized to the $LiMnO_2$, the compound had a formula $Li_{1.14}Co_{0.28}Mn_{0.51}O_2$. The Rietveld refinement result confirmed that the sample prepared with a weight ratio of $Co_{0.35}Mn_{0.65}O_2$ to $LiOH \cdot H_2O$ was 1:4, with a composition of $Li_{0.93}[L_{0.21}Co_{0.28}Mn_{0.51}]O_2$, which agreed with the ICP-MS results (Fig. 3). We assumed that Li was in the 3a sites, Co^{3+}, Mn^{4+} and Li^+ were in the 3b sites, and oxygen was in the 6c sites. Since the radii of the Co^{3+} (0.542 Å) and Mn^{4+} (0.53 Å) were much smaller than that of Li^+ (0.76 Å), no Co^{3+}, Mn^{4+} were expected to be in the 3a sites [23] (sample C).

Fig. 4 shows SEM (a–c) and TEM images (d) of samples A, B, and C, and the octahedral shapes of the particles was indicative of the formation of the typical spinel phase (Fig. 4a). By increasing the temperature and LiOH concentrations, particles with plate shapes (sample C) became dominant and completely changed into hexagonally shaped nanoplates with a thickness of 20 nm (see Fig. 4c and d). Fig. 5 shows Mn K-edge XANES spectra of samples A, B, and C and spectra of the reference materials. The peak features are very sensitive to the oxidation state of the central Mn atom, the bond covalency, and the local structure around Mn atom. All spectra exhibited two pre-edge peaks, A1 and A2, which are associated with the quadruple allowed $1s \rightarrow 3d$ (e_g) and $1s \rightarrow 3d$ (t_{eg}) transitions, respectively [24,25]. The two shoulder peaks B1 and B2 are typical features for spinel $LiMn_2O_4$, of which the shoulder C corresponds to the $1s \rightarrow 4Pz$ transition of Mn^{3+} cations with a shakedown process, followed by the ligand to metal charge transfer (LMCT). The pre-edge peaks shifted to higher energies are indicative of the increase in the Mn oxidation state. Overall, the oxidation states of samples A and B were 3.5+ and sample C was 4+. In addition, the intermediate bump at 6552 eV was predominant for samples B

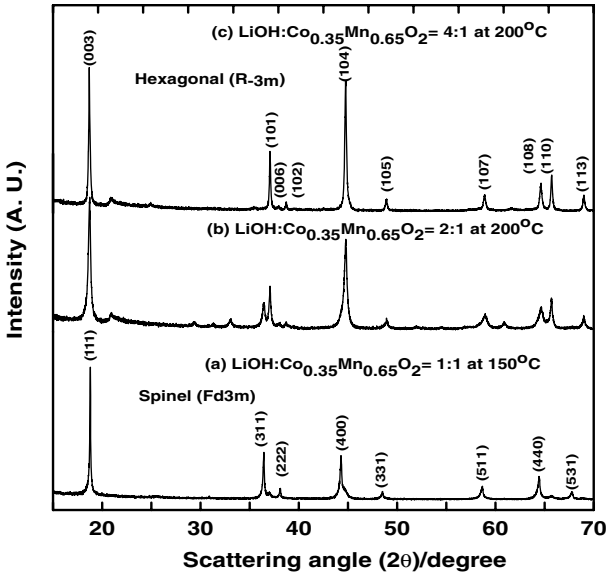

Fig. 2. XRD patterns of the $Li_xCo_{0.35}Mn_{0.65}O_{2+z}$ prepared at different $LiOH \cdot H_2O$ and $Co_{0.35}Mn_{0.65}O_2$ concentrations ($Co_{0.35}Mn_{0.65}O_2$: $LiOH \cdot H_2O = 1{:}1$, 1:2, and 1:4) (wt%) at 150 °C and 200 °C.

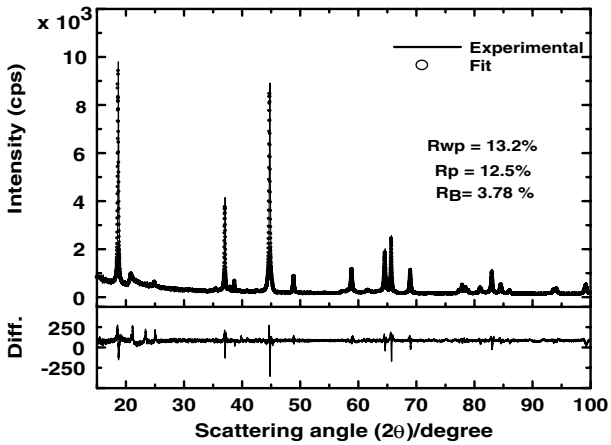

Fig. 3. A Rietveld refinement of $Li_{1.5}Co_{0.35}Mn_{0.65}O_{5.15}$. When normalized to the $LiMnO_2$,the compound had formula $Li_{0.93}[Li_{0.21}Co_{0.27}Mn_{0.51}]O_2$.

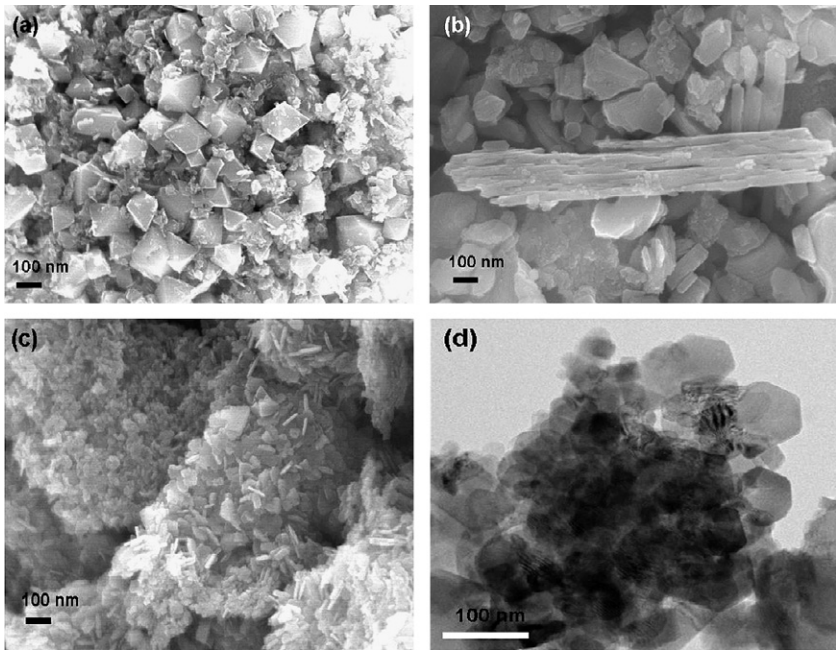

Fig. 4. SEM (a–c) and TEM images (d) of different LiOH · H_2O and $Co_{0.35}Mn_{0.65}O_2$ concentration (weight ratio of $Co_{0.35}Mn_{0.65}O_2$ to LiOH · H_2O) (a) sample A, (b) sample B, and (c) and (d) sample C.

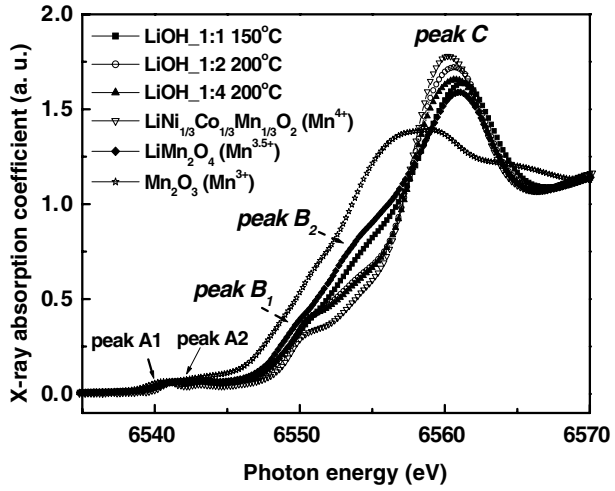

Fig. 5. Mn K-edge XANES spectra of the samples A, B, and C and the spectra of reference materials.

and C, similar to $LiNi_{1/3}Co_{1/3}Mn_{1/3}O_2$, which indicates that the connectivity between the MnO_6 octahedra in the structure is highly ordered [26].

Fig. 6a and b shows the voltage profiles of sample C between 2 and 4.8 V at a rate of 0.1C, as well as the corresponding ex situ XRD patterns at designated voltages (a–f). During cycling, the original layered structure was maintained. The Rietveld results of the pristine sample showed that the lattice constants a, c, and their ratio c/a were 2.8427(2), 14.245(1), and 5.01, respectively, after charging to 4.8 V, $a = 2.8679(5)$ and $c = 14.291(3)$ ($c/a = 4.98$). After fully discharging to 2.7 V (g), a layered phase with a c/a ratio similar to that of the pristine sample (before cycling) was maintained ($a = 2.8582(2)$, $c = 14.294(2)$, $c/a = 5.00$).

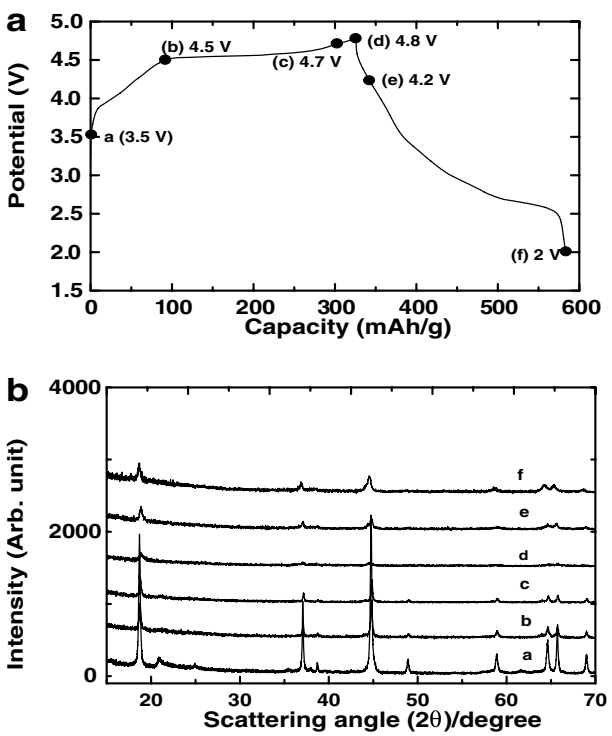

Fig. 6. Voltage profiles of sample C between 2 and 4.8 V at a rate of 0.1C, and the corresponding ex situ XRD patterns at designated voltages (a–f).

According to the previous study on $Li[Li_{1-x-y}Ni_xMn_y]O_2$, the large capacity plateau was related to the oxygen loss from the structure, thus forming an oxygen deficient $[Li_{1-x-y}Ni_xMn_y]O_{2-z}$ phase [27]. Fig. 7a shows voltage profiles of sample C, corresponding to $Li_{0.93}[L_{0.21}Co_{0.27}Mn_{0.51}]O_2$. The $Li_{0.93}[L_{0.21}Co_{0.27}\ Mn_{0.51}]O_2$ cathode showed a first

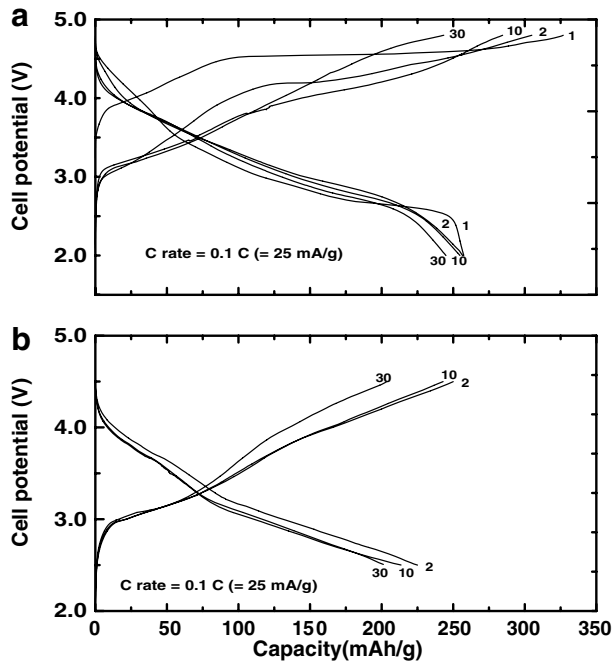

Fig. 7. Voltage profiles of sample C, corresponding to $Li_{0.93}[Li_{0.21}Co_{0.28}Mn_{0.51}]O_2$, at a rate of 0.1C (=25 mA/g) between (a) 2 and 4.8 V and (b) 2.5 and 4.5 V. In Fig. 7 b, the cell was cycled between 4.8 and 2 V for the first cycle, and continued to cycle between 2.5 and 4.5 for the rest of the cycles.

discharge capacity of 258 mAh/g with an irreversible capacity ratio of 20%. The capacity retention after 30 cycles was 95% and did not show the plateau at 3 V at that cycle, indicating the spinel phase had not formed after extended cycling. On the other hand, the fact that $Li[Co_{0.17}Li_{0.26}Mn_{0.57}]O_2$ exhibited a clear plateau at 3 V after 20 cycles indicated that the amount of Co content required to prevent a spinel transition may be over 20 mole % of the transition metal [21]. After first cycling between 2 and 4.8 V, when subsequent cycles were limited between 4.5 and 2.5 V, the discharge capacities after 2nd and 30th cycles was 225 mAh/g and 200 mAh/g, respectively (Fig. 7b).

Fig. 8 exhibits rate performance of the $Li_{0.93}[L_{0.21}Co_{0.28}Mn_{0.51}]O_2$ cathodes between 0.1 C and 4C rate under electrode density of 25 mg/cm^2 between 2 and 4.8 V and capacity retention at 4 C was 84%, compared with 0.1 C (=25 mA/g). In addition, the cathode shows good capacity retention at extended 4C rate cycling, followed by full capacity recovery when C rate reduces to 0.1 C. This result is superior to previous nanocrystalline $Li[Li_{0.2}Ni_{0.2}Mn_{0.6}]O_2$ cathode with mixed particle sizes with 80–200 nm and 1–20 μm that showed 43% capacity retention when the current increased from 20 mA/g to 800 mA/g (this material was prepared by a combustion method) [22]. The improvement of the $Li_{0.93}[L_{0.21}Co_{0.28}Mn_{0.51}]O_2$ cathode is believed to be due to its nanoplate-like morphology with a thickness of 20 nm that facilitates the shorter Li diffusion length, compared with conventional nanocrystalline particles prepared by combustion method [22].

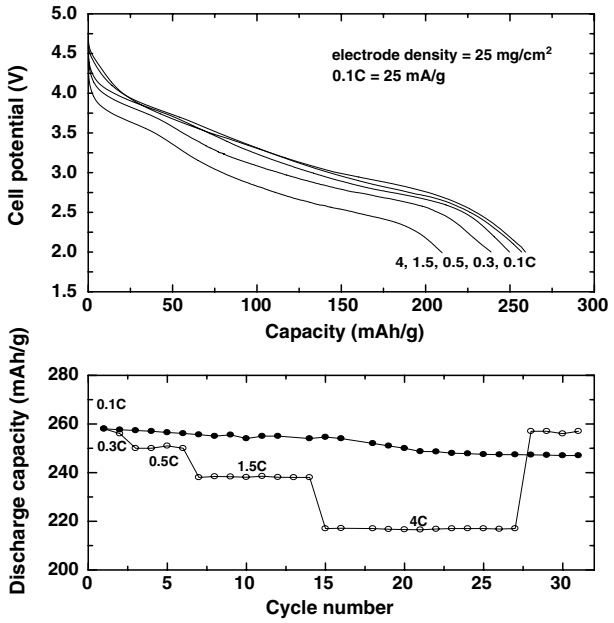

Fig. 8. Plots of the voltage profiles of $Li_{0.93}[Li_{0.21}Co_{0.28}\ Mn_{0.51}]O_2$ cathodes at different C rates, 0.1, 0.3, 0.5, 1.5, and 4C and cycle number vs. discharge capacity at 0.1, 0.3, 0.5, 1.5, and 4C rates.

4. Conclusions

We prepared well ordered, layered $Li_{0.93}[Li_{0.21}Co_{0.28}Mn_{0.51}]O_2$ cathode powders from a hydrothermal reaction at 200 °C using K-birnessite as a precursor. In contrast to the conventional hydrothermal method using $NaMnO_2$, this method used layered $Co_{0.35}Mn_{0.65}O_2$ obtained from cationic exchange with K-birnessite. Although this cathode showed a high discharge capacity of 258 mAh/g and relatively good capacity retention. In addition, nanoplate-like morphology facilitated much improved rate performance even at 4C rate, showing 84%.

Acknowledgements

The authors acknowledge the Pohang Light Source (PLS) for the XAS measurements. This work was supported by University ITRC Research Project.

References

[1] C. Fouassier, C. Delams, P. Hagenmuller, Mater. Res. Bull. 10 (1975) 443.
[2] M.H. Rossouw, D.C. Liles, M.M. Thackeray, J. Solid State Chem. 104 (1993) 464.
[3] M.M. Thackeray, J. Electrochem. Soc. 142 (1995) 2558.
[4] F. Leroux, D. Guyomard, Y. Piffard, Solid State Ionics 80 (1995) 299.
[5] A.R. Armstrong, P.G. Bruce, Nature 381 (1996) 499.
[6] A.R. Armstrong, R. Gitzendanner, A.D. Robertson, P.G. Bruce, Chem. Commun. (1998) 1833.
[7] P.G. Bruce, A.R. Armstrong, R.L. Gitzendanner, J. Mater. Chem. 9 (1999) 193.
[8] F. Capitaine, P. Gravereau, C. Delmas, Solid State Ionics 89 (1996) 197.
[9] M. Tabuchi, K. Ado, H. Kobayashi, H. Kageyama, A. Kondo, R. Kanno, J. Electrochem. Soc. 145 (1998) L49.

[10] D. Larcher, M.R. Palacin, G.G. Amatucci, J.-M. Tarascon, J. Electrochem. Soc. 144 (1997) 408.
[11] Y. Xu, Q. Feng, K. Kajiyoshi, K. Yanagisawa, X. Yang, Y. Makita, S. Kasaishi, K. Ooi, Chem. Mater. 14 (2002) 3844.
[12] S. Ching, D.J. Petrovay, M.L. Jorgensen, Inorg. Chem. 36 (1997) 883.
[13] R. Chen, P. Zavalij, M.S. Whittingham, Chem. Mater. 8 (1996) 1275.
[14] S. Ching, J.A. Landrigan, M.L. Jorgensen, Chem. Mater. 7 (1995) 1604.
[15] M. Tsuda, H. Arai, Y. Sakurai, J. Power Sources 110 (2002) 52.
[16] D.C. Golden, J.B. Dixon, C.C. Chen, Clay. Clay Miner. 34 (1986) 511.
[17] Q. Feng, H. Kanoh, Y. Miyai, K. Ooi, Chem. Mater. 7 (1995) 1226.
[18] P.L. Goff, N. Baffier, S. Bach, J.P. Pereira-Ramos, Mater. Res. Bull. 31 (1996) 63.
[19] Y.J. Park, M.G. Kim, Y.-S. Hong, X. Wu, K.S. Ryu, S.H. Chang, Solid State Commun. 127 (2003) 509.
[20] Z. Lu, J.R. Dahn, J. Electrochem. Soc. 149 (2002) A815.
[21] Y.J. Park, M.G. Kim, Y. -S. Hong, X. Wu, K.S. Ryu, S.H. Chang, J. Electrochem. Soc. 151 (2004) A720.
[22] Y.-S. Hong, Y.J. Park, K.S. Ryu, S.H. Jang, M.G. Kim, J. Mater. Chem. 14 (2004) 1424.
[23] R.D. Shannon, C.T. Prewitt, Acta Crystallogr., Sect. A A32 (1976) 751.
[24] W.-S. Yoon, K.-B. Kim, M.-G. Kim, M.-K. Lee, H.-J. Shin, J.-M. Lee, J. Electrochem. Soc. 149 (2002) A1305.
[25] W.-S. Yoon, K.-B. Kim, M.-G. Kim, M.-K. Lee, H.-J. Shin, J.-M. Lee, C.-H. Yo, J. Phys. Chem. B 106 (2002) 2526.
[26] M.G. Kim, H.J. Shin, J.-H. Kim, S.-H. Park, Y.-K. Sun, J. Electrochem. Soc. 152 (2005) A1320.
[27] A.R. Armstrong, M. Holzapfel, P. Novak, C.S. Johnson, S.-H. Kang, M.M. Thackeray, P.G. Bruce, J. Am. Chem. Soc. 128 (2006) 8694.